ADVANCED HEALTHCARE MATERIALS
www.advhealthmat.de

Graphene Field-Effect Transistors for the Sensitive and Selective Detection of *Escherichia coli* Using Pyrene-Tagged DNA Aptamer

Guangfu Wu, Ziwen Dai, Xin Tang, Zihong Lin, Pik Kwan Lo, Meyya Meyyappan,* and King Wai Chiu Lai**

This study reports biosensing using graphene field-effect transistors with the aid of pyrene-tagged DNA aptamers, which exhibit excellent selectivity, affinity, and stability for *Escherichia coli* (*E. coli*) detection. The aptamer is employed as the sensing probe due to its advantages such as high stability and high affinity toward small molecules and even whole cells. The change of the carrier density in the probe-modified graphene due to the attachment of *E. coli* is discussed theoretically for the first time and also verified experimentally. The conformational change of the aptamer due to the binding of *E. coli* brings the negatively charged *E. coli* close to the graphene surface, increasing the hole carrier density efficiently in graphene and achieving electrical detection. The binding of negatively charged *E. coli* induces holes in graphene, which are pumped into the graphene channel from the contact electrodes. The carrier mobility, which correlates the gate voltage to the electrical signal of the APG-FETs, is analyzed and optimized here. The excellent sensing performance such as low detection limit, high sensitivity, outstanding selectivity and stability of the graphene biosensor for *E. coli* detection paves the way to develop graphene biosensors for bacterial detection.

1. Introduction

Simple and rapid identification of pathogens such as *Escherichia coli* (*E. coli*) is at the core of microbial diagnosis, human health, environmental analysis, and food safety.[1] The most conventional methods for bacteria detection are based on bacterial culturing and phenotypic/metabolic fingerprinting.[2] Although they are reliable and accurate, the processes are time-consuming and complicated, which require several days to obtain the results. In addition, the lack of electrical signal output may hinder miniaturization attempts for wide use in consumer applications from the perspective of simple and rapid detection. In this regard, biosensors that can convert the probe-target interaction into a detectable electrical signal are preferable. Recently, solution-gated graphene field-effect transistors (G-FETs) have been demonstrated as a platform for biodetection.[3–6] Usually, surface functionalization is considered to control device's signal. One recent study has indicated the correlation between aromatic molecule and buffer solution during functionalization.[7] Graphene has excellent properties such as high carrier mobility, outstanding electronic conductivity, and large specific area that make it a promising sensing material for the development of biosensors.[8] The gate-dependent carrier mobility of the G-FET-based biosensor provides an excellent avenue to achieve electrical detection with high performance.

To date, antibody-modified G-FETs have been employed to develop biosensors for bacterial detection.[9,10] However, antibody production suffers from batch-to-batch variations and antibodies are difficult to store and transport, which limit their applications in the field of biosensing. The discovery of aptamers that can specifically interact with the target opens up possibilities to develop bacterial biosensors with good sensitivity, selectivity, and stability. It has been confirmed that aptamers are comparable to antibodies when they are used as the sensing probes.[11] Aptamer was first isolated using the SELEX (systematic evolution of ligands by exponential amplification) method.[12,13] Recently, there has been growing interest in developing various aptamers as sensing probes[14–18] as they possess advantages such as facile modification, good stability, and high affinity toward various species from ions to whole cells.[19]

We report the development of aptamer-modified G-FETs (APG-FETs) for *E. coli* detection. In the specific area of bacterial detection, excellent sensitivity, selectivity, and stability are achieved by taking advantage of aptamer and using the concept

G. F. Wu, Dr. X. Tang, Z. H. Lin, Dr. K. W. C. Lai
Department of Mechanical and Biomedical Engineering
Centre for Robotics and Automation
City University of Hong Kong
83 Tat Chee Ave, Kowloon Tong, Hong Kong SAR, P. R. China
E-mail: kinglai@cityu.edu.hk
Z. W. Dai, Dr. P. K. Lo
Department of Biology and Chemistry
City University of Hong Kong
83 Tat Chee Ave, Kowloon Tong, Hong Kong SAR, P. R. China
E-mail: peggylo@cityu.edu.hk
Dr. M. Meyyappan
NASA Ames Research Center
Moffett Field, CA 94035, USA
E-mail: m.meyyappan@nasa.gov
The ORCID identification number(s) for the author(s) of this article can be found under https://doi.org/10.1002/adhm.201700736.

DOI: 10.1002/adhm.201700736

of modified G-FET. A pyrene tag was used to link the DNA aptamer and graphene. The fabricated G-FETs were modified with the sensing probe, namely, the pyrene-tagged DNA aptamer (PTDA), to achieve specific electrical detection of *E. coli*. The increase of the hole carrier density in the probe-modified graphene due to the attachment of *E. coli* is analyzed in this study to obtain an optimized electrical response. The binding of *E. coli* causes a conformational change of the aptamer. The conformational change brings the negatively charged *E. coli* close to the graphene surface, thus allowing for the efficient *E. coli*-induced electrostatic gating. The high carrier mobility of the APG-FETs is tuned by the gate voltage, leading to the highly efficient *E. coli*-induced carrier (holes) collection in graphene. Besides, the selectivity and stability of the APG-FETs for *E. coli* detection is also studied systematically.

2. Results and Discussion

2.1. Design and Fabrication of the Pyrene-Tagged Aptamer-Modified G-FETs

The G-FET contains two metal electrodes, namely, the source and drain electrodes, and the graphene layer serves as the conducting channel bridging the contact electrodes. Si wafer with a 300 nm oxidation layer was used as the substrate. The patterned graphene (120 µm × 100 µm) was assembled with the ***FET structure. Then the source and drain electrodes were insulated by SU-8 photoresist. Details on graphene patterning and G-FET fabrication can be found in the Supporting Information. The active sensing area of graphene was about 100 µm (w) × 100 µm (l). The G-FET was functionalized with the PTDA to realize the desired specific detection. As shown in **Figure 1**, the as-prepared G-FET was incubated with the PTDA (0.93×10^{-6} M in deionized water) for 4 h at room temperature (25 °C). This particular aptamer was proved to possess high affinity and specificity toward *E. coli* 8739, which was ascribed to the specific binding between the aptamer and an out membrane protein or the lipopolysaccharide of *E. coli*.[20] In this study, it was coupled into the G-FET to develop a new biosensor for electrical detection of bacteria. To anchor the PTDA onto the surface of graphene, the pyrene tag (pyrene phosphoramidite) was coupled into the 5′-end of the DNA aptamer with a spacer of four thymines (T) during the DNA aptamer synthesis process. The pyrene tag was successfully characterized by ^{1}H NMR, ^{13}C NMR, ^{31}P NMR, and ESI-MS, and the PTDA was confirmed with MALDI-TOF MS. (Detailed information is given in the Supporting Information.)

2.2. Theoretical Model and Optimization

Understanding the change of the carrier density in the probe-modified graphene due to the attachment of *E. coli* is the key to improving the sensing performance of the G-FETs. The adsorption of charged targets in a solution-gated G-FET can cause an increase or decrease of the source–drain current (ΔI_{ds}) during real-time electrical monitoring. In our study, the binding of negatively charged *E. coli* induces holes in the graphene channel, causing the device current to increase. The current modulation is expressed as a function of the change in the carrier density (Δn) in the graphene channel, which is proportional to the number of targets (N) attached on the surface of graphene[21,22]

$$\Delta I_{ds} = \frac{w}{l} \cdot e \cdot \mu \cdot V_{ds} \cdot \Delta n \propto N \quad (1)$$

where w is the width of the graphene channel; l is the length of the graphene channel; e is elementary charge (1.602×10^{-19} C); μ is the carrier mobility; V_{ds} is the source–drain voltage. Both V_{ds} and w/l ratio have been known to affect the electronic properties of G-FETs.[23] First, a low V_{ds} allows low power operation of the G-FETs, which ensures no chemical reactions on the surface of the graphene channel. Second, more wrinkles and vestiges are possible on the graphene channel with large w/l ratios, which deteriorate the carrier mobility of the G-FETs. Besides, more contamination can be introduced to the graphene sample with large size.[24] Both w/l ratio and V_{ds} were kept as constants for the real-time electrical monitoring in this study and the carrier mobility μ was chosen as the most important parameter to assess the sensing performance. The carrier mobility, which is

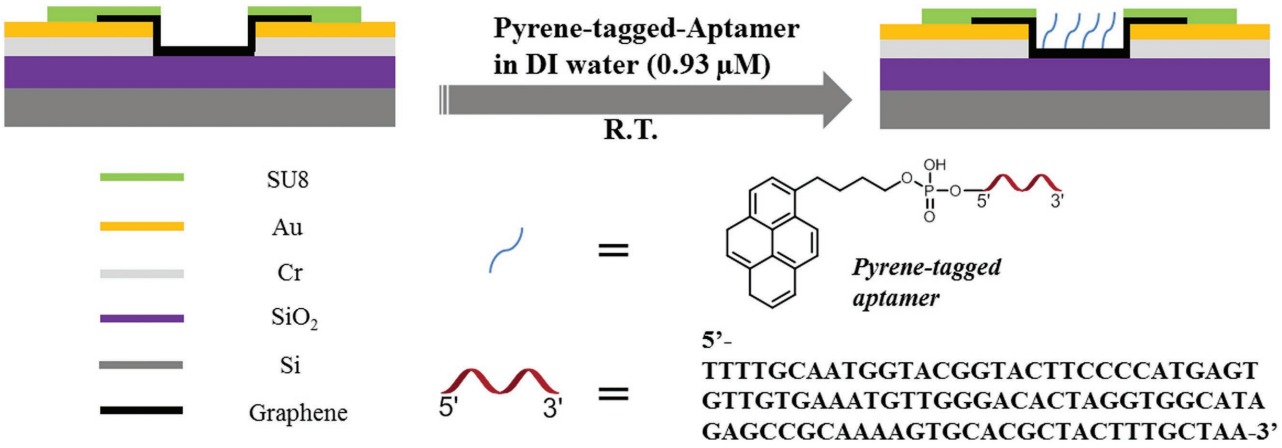

Figure 1. Schematic illustration of the PTDA-modified G-FET.

a measure of the carrier transport in a material, is an essential characteristic of the G-FET and high carrier mobility suggests that the carriers (hole or electron) can be collected by the electrodes efficiently. The carrier mobility is determined by the gate voltage when other conditions are kept constant, which is given by[25]

$$\mu = \frac{\partial I_{ds}}{\partial V_g} \cdot \frac{l}{w} \cdot \frac{1}{C_{TG} \cdot V_{ds}} \quad (2)$$

where C_{TG} is the total gate capacitance, which is defined by the concentration of the electrolyte.[26] The electrolyte with a suitable concentration makes the probe–target interaction unscreened. The detailed carrier mobility calculations can be found in the Supporting Information. In this study, the gate voltage that gives the largest carrier mobility is chosen to obtain the electrical response of the graphene devices to *E. coli*.

2.3. Characterizations of the PTDA Functionalization

The functionalization of the G-FETs with the PTDA was characterized by electrical measurements. The G-FETs were fabricated on the Si chip and each chip consisted of four single G-FET devices as shown in **Figure 2**a. The electrical measurements were recorded on a Keysight B1500 semiconductor analysis system assembled with a micromanipulation stage. To obtain the transfer characteristics of the APG-FETs, the measurements were performed with a V_{ds} of 0.1 V to avoid possible chemical reaction on the surface of the graphene channel.[23] In Figure 2b, a representative G-FET exhibits ambipolar characteristics (black line) and the voltage at the Dirac point (V_{DP}) is 0.24 V, which indicates that the G-FETs operate in the p-type region. After the PTDA functionalization, the V_{DP} shifts slightly from 0.24 to 0.225 V (red line) because the PTDA is negatively charged DNA chain, which donates electrons to graphene causing the n-doping effect on graphene. This phenomenon is consistent with previous observations.[27] The transfer characteristics of ten graphene transistors for the PTDA functionalization were measured and the reproducibility of the devices was analyzed as given in the Supporting Information. The small fluctuations of V_{DP} (0.24 ± 0.003 V) for these G-FETs suggest excellent repeatability of the fabrication of the graphene devices. The V_{DP} of these G-FETs after the PTDA treatment is 0.225 ± 0.004 V, which implies the excellent repeatability of the PTDA functionalization.

Atomic force microscopy (AFM) was employed to examine the PTDA functionalization on graphene as well. The AFM

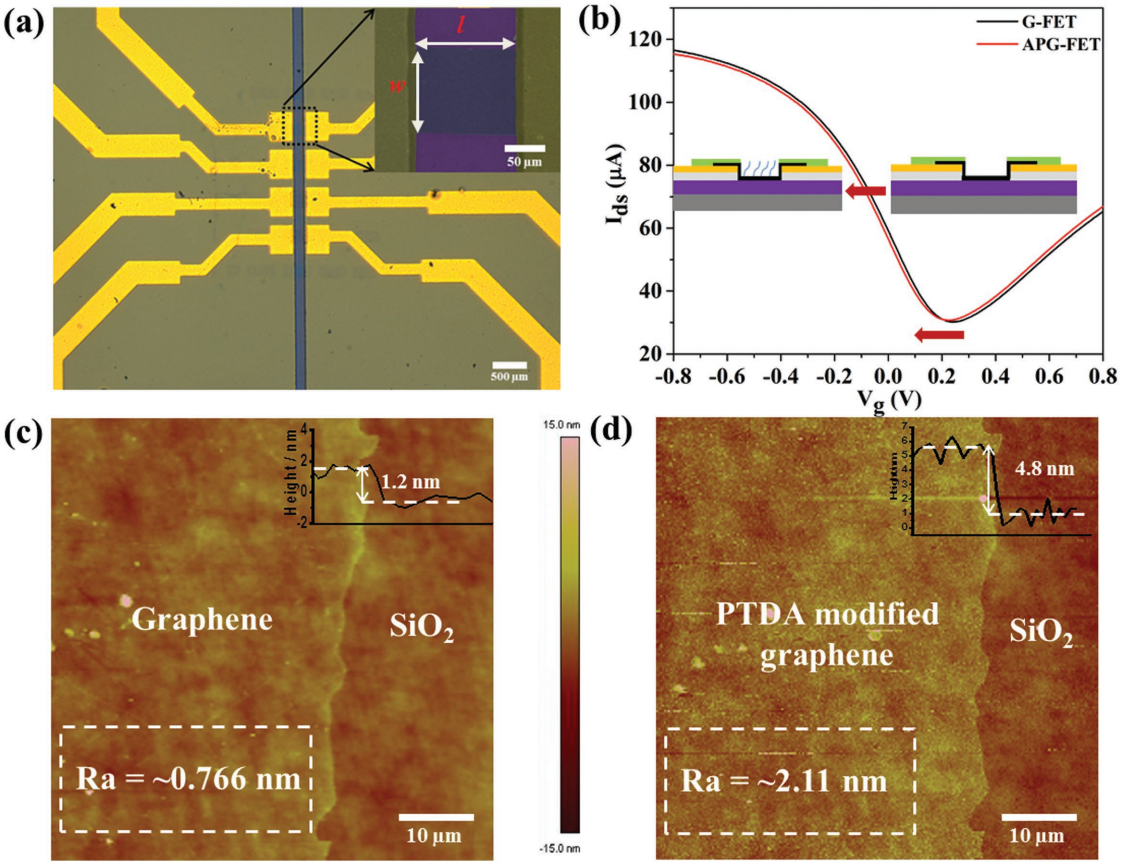

Figure 2. Characterization of graphene before and after the PTDA functionalization. a) Optical microscope image of Si chip with four G-FETs. Inset: The scanning electron microscope (SEM) image of the single G-FET. The sensing area was about 100 µm (*w*) × 100 µm (*l*). b) Transfer characteristics of a typical graphene transistor before (black line) and after (red line) the PTDA treatment (APG-FET). c) AFM topography of bare graphene. d) AFM topography of the aptamer-modified graphene.

scanning images and the thickness of graphene before and after the PTDA functionalization are shown in Figure 2c,d. The thickness of the bare graphene is estimated to be 1.2 nm, indicating a monolayer graphene. This value is larger than the theoretical thickness of graphene (0.34 nm), which is due to some adsorbed molecules on the graphene surface or on the interface between graphene and the substrate during the transfer process.[28] After the surface functionalization of graphene, this value increases to 4.8 nm. The height of the PTDA is 3.6 nm, which is consistent with the size of the aptamers in other studies.[29,30] The surface roughness of graphene (R_a) exhibits a significant increase from 0.766 to 2.11 nm after the PTDA functionalization, which is attributed to the flexibility of the aptamer molecule. This observation further proves the attachment of the aptamer on the graphene surface.

2.4. Electrical Detection of *E. coli* and Gate-Dependent Carrier Mobility

We then investigated the electrical performance of the APG-FETs for *E. coli* detection. In this study, the gate voltage was applied to the graphene channel via an Ag/AgCl electrode, which was immersed into the electrolyte. As shown in **Figure 3**, the addition of high concentration of *E. coli* (10^6 CFU mL^{-1}) causes a significant right shift of the transfer characteristics. The current response ranges from 2% to 13% (detailed current response calculation can be found in the Supporting Information). The current response of 13% to *E. coli* (10^6 CFU mL^{-1}) at V_g = 0.04 V is one of the largest responses compared with previous studies. Antibody-modified G-FET exhibited a response of 12% upon exposure to *E. coli* (10^5 CFU mL^{-1}).[9] Antibody-modified reduced graphene oxide FET exhibited a response of 7.3% to *E. coli* (10^5 CFU mL^{-1}).[10] In another study, the antimicrobial peptides-modified G-FET exhibited a larger response of 20% to much higher *E. coli* concentration (10^7 CFU mL^{-1}).[31] These comparisons indicate that our

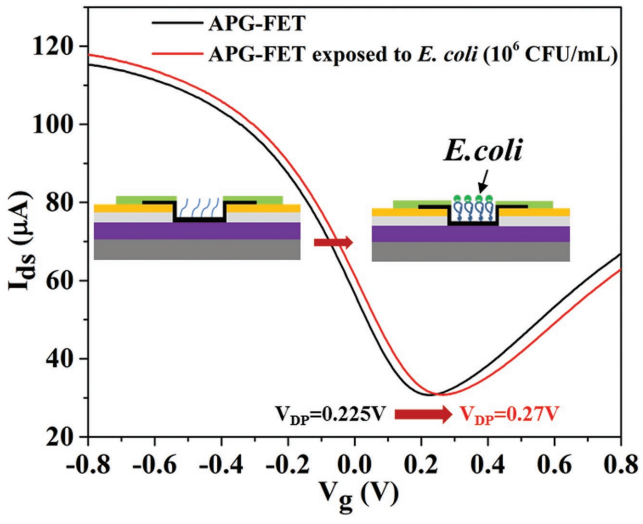

Figure 3. The transfer characteristics of the APG-FET (black) and 10^6 CFU mL^{-1} of *E. coli*-treated APG-FET (red). Upon exposure to *E. coli*, the V_{DP} of the APG-FET shifted from 0.225 to 0.27 V.

biosensor using aptamer and G-FET can be used for *E. coli* detection with good current response. The V_{DP} exhibits a right shift from 0.225 to 0.27 V, implying a p-doping effect of *E. coli* on graphene. Ten APG-FET devices with similar electrical properties (V_{DP} = 0.225 ± 0.004 V) were exposed to *E. coli* (10^6 CFU mL^{-1}), and the V_{DP} exhibited obvious and consistent right shift to 0.27 ± 0.004 V as shown in Figure S10 (Supporting Information). The right shift of V_{DP} is explained by the *E. coli*-induced electrostatic gating mechanism (**Figure 4**a,b). The surface of *E. coli* is negatively charged in 0.01 × phosphate buffered saline (PBS) buffer (pH = 7.2) due to the deprotonation of both carboxylates and phosphates.[32] Since graphene is electrically grounded, the negatively charged *E. coli* imposes an external electric field with direction toward the electrolyte. The external electric field shifts the Fermi level of graphene downward. Therefore, when the negatively charged *E. coli* is added and captured by the aptamer PTDA, the hole carrier density in graphene is increased. As a result, the right shift of the Dirac point (p-doping) is observed. It is noteworthy that the aptamer undergoes a conformational change[33,34] when the aptamer binds with *E. coli* as shown in Figure 4c. The *E. coli*-induced conformational change brings the negatively charged *E. coli* close to graphene surface, increasing the hole carrier density efficiently in graphene. Therefore, a significant increase of the electrical current is observed when the APG-FET is exposed to *E. coli*. The possible structure of this DNA aptamer that binds with *E. coli* is predicted using Mfold.[35] As shown in Figure 4d, we speculate that the particular structure in red color may play a key role in binding with *E. coli* because it shares the same sequence of other aptamers that show high affinity toward *E. coli* in the previous study.[20] (Detailed analysis of the aptamers in binding with *E. coli* can be found in Figure S13 in the Supporting Information.)

To investigate the gate-dependent response of the APG-FETs, the changes in the I_{ds} caused by the addition of *E. coli* are summarized by subtracting the black line in Figure 3 from the red line. The relationship between the current change of the graphene device and the gate voltage is plotted in **Figure 5**a. The results show that the sign and the magnitude of the response are gate dependent. In the left branch (the region marked in red), the additional holes induced by *E. coli* enhance the conductivity of the graphene devices, leading to the positive response. While in the right branch (the region marked in blue), the *E. coli*-induced holes counteract the electrons in graphene, causing the negative response. The two maximum responses are noted at the gate voltage of 0.04 V in the left branch and 0.59 V in the right branch.

We speculate that the gate-dependent response is related to the carrier mobility of graphene, as the electrical response is proven to be proportional to the carrier mobility based on Equation (1).[20] The gate-dependent carrier mobility was extracted from Equation (2), as shown in Figure 5b. The positive and negative values are defined for hole and electron, respectively. Obviously, the magnitude of the carrier mobility is gate-dependent and a maximum hole (electron) mobility of 1030.99 cm^2 V^{-1} s^{-1} (459.21 cm^2 V^{-1} s^{-1}) is obtained at the gate voltage of 0.04 V (0.595 V), which matches well with the gate voltages at the maximum electrical response. The detailed carrier mobility calculations can be found in the supporting

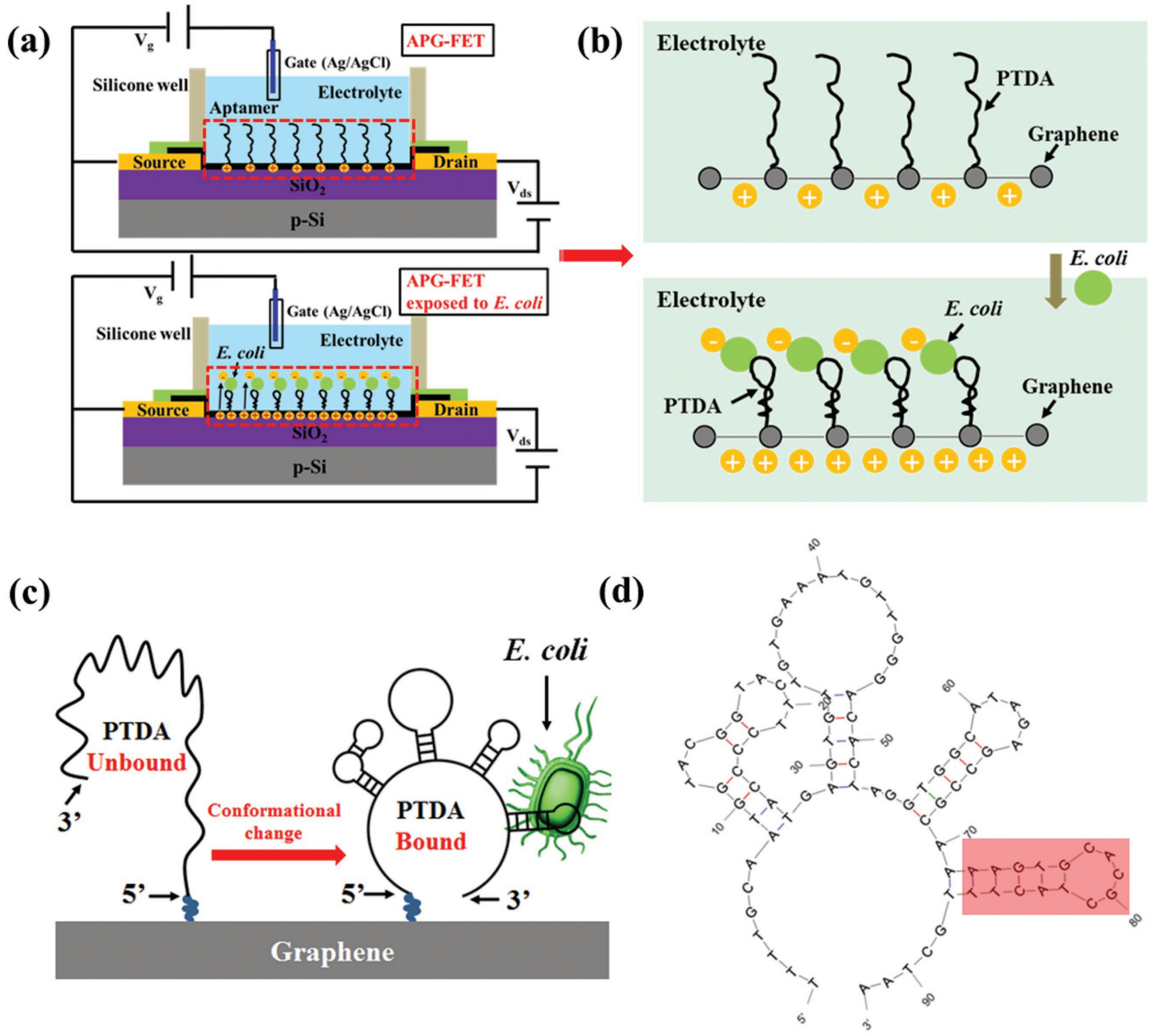

Figure 4. The sensing mechanism of the APG-FET biosensors for *E. coli* detection. a) The APG-FET biosensor setup and the binding of *E. coli*. b) Illustration of the aptamer structure change and the change of the charge distribution induced by the binding of the negatively charged *E. coli*. c) The *E. coli*-induced conformational change of the aptamer. d) The prediction of the secondary structure of the aptamer using Mfold based on the surface free energy minimization algorithm. The red rectangle represents the possible part that makes a key contribution to the binding with *E. coli*.

information. Therefore, the device performance can be optimized by controlling the gate voltage as seen from the results above.

2.5. Real-Time Current Monitoring of the APG-FETs for *E. coli* Detection and Quantitative Analysis

To quantitatively evaluate the concentration-dependent response of the biosensors toward the bacteria, the real-time current recording of the as-prepared APG-FETs was performed with successive addition of *E. coli* at different concentrations. The real-time measurements were performed with a V_{ds} of 0.05 V to avoid possible oxidation reaction on the graphene surface. The 0.01 × PBS buffer was used as the electrolyte and the graphene devices were gated at the optimal gate voltage of 0.04 V. The crude bacterial culturing solution was directly diluted with 0.01 × PBS buffer to different concentrations. Since the bacterial culture medium and the PBS buffer are involved in the bacterial detection, the electrical signals of the APG-FETs upon addition of these two solutions were investigated as the control group. As shown in **Figure 6**a (black line), negligible changes in the current of the APG-FETs are seen after the addition of the culture medium and the PBS buffer, which indicates that both these solutions have no obvious effect on the devices. Then we measured the electrical current of the APG-FET devices exposed to *E. coli* at different concentrations of 10^2, 10^3, 10^4, 10^5, and 10^6 CFU mL^{-1}. As shown in Figure 6a (red line), the APG-FETs show a

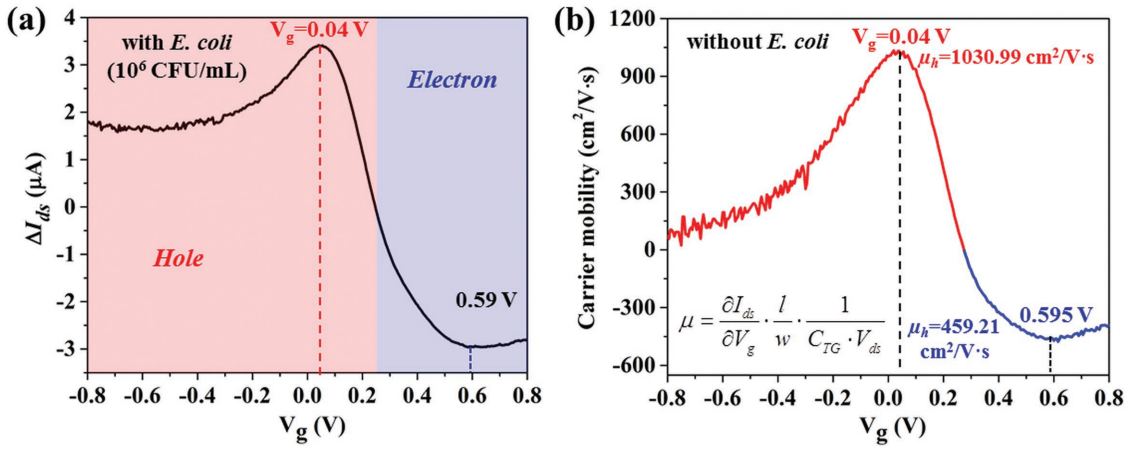

Figure 5. a) The current change of the APG-FET after the addition of *E. coli* solution (10^6 CFU mL^{-1}), which was obtained by subtracting the black line from the red line in Figure 3. b) The carrier mobility of graphene at different gate voltages obtained from the transfer curve (black line) in Figure 3, which represents the carrier mobility of the pyrene-tagged DNA-aptamer-modified graphene without the presence of *E. coli*.

concentration-dependent response. The source–drain current I_{ds} exhibits a stepwise increase at each concentration. The detection limit of the APG-FETs is 10^2 CFU mL^{-1}, which is comparable with previous studies as shown in **Table 1**. The exposure of the graphene devices to this concentration of *E. coli* causes an obvious increase in device current within about a minute (72 s) as shown in the inset of Figure 6a; this is faster than some of the reported methods for bacterial detection such as the flow cytometry, the polymerization chain reaction (PCR) test, fluorescence method, and antibody-modified G-FET, as shown in Table 1. Besides, the sensitivity at the detection limit (10^2 CFU mL^{-1}) was about 2.5×10^{-3} μA per (CFU mL^{-1}). This value is at the same order when compared with previous study as shown in Table 1. These results further indicate that our biosensor using the aptamer and G-FET is a promising platform for bacterial detection.

The source–drain current I_{ds} increases significantly with *E. coli* concentration from 10^2 to 10^5 CFU mL^{-1}, and then the signal saturates gradually for concentrations above 10^5 CFU mL^{-1}. The maximum response is obtained (the maximum net change in source–drain current $\Delta I_{ds,\,max}$ = 1.686 μA) at an *E. coli* concentration of 10^6 CFU mL^{-1}. We idealize that the whole surface of the graphene is occupied by *E. coli* and all of these *E. coli* cells contribute to the increase of the device current. The active sensing area of graphene is about 100 μm × 100 μm and the size of a single *E. coli* is about 1.5 μm × 0.5 μm.[39] Therefore, the largest number of *E. coli* reaching the surface of the aptamer-modified graphene is estimated to be ≈13 333. Based on Equation (1), the smallest number of carriers (holes) induced per *E. coli* is calculated as 1531. The detailed carrier density evaluation can be found in the Supporting Information.

We then investigated the affinity of the aptamer toward *E. coli* by estimating the dissociation constant. The relationship between the electrical current of the APG-FET devices and the concentration of *E. coli* can be interpreted by the Langmuir adsorption isotherm[40]

$$\Delta I_{ds} = \frac{\Delta I_{ds,max} \cdot C_{E.coli}}{K_D + C_{E.coli}} \tag{3}$$

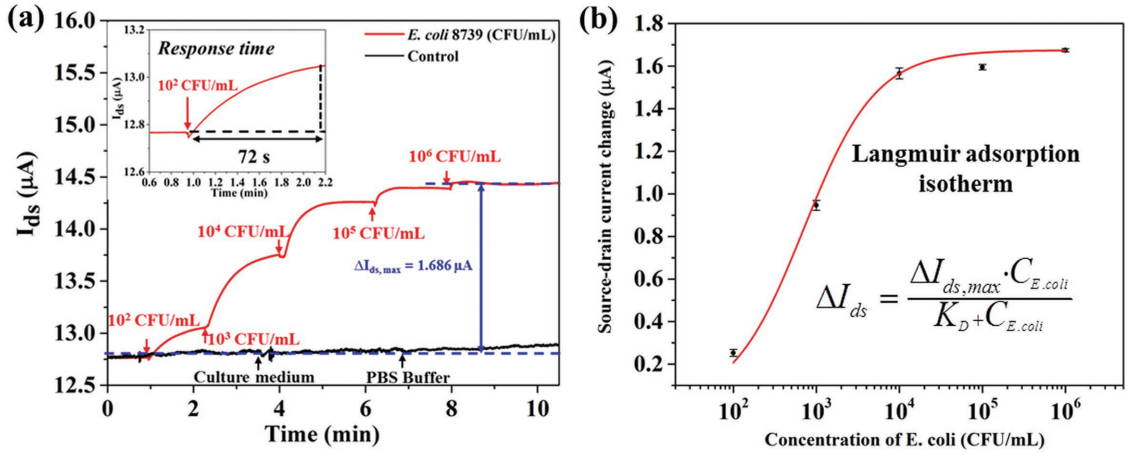

Figure 6. The performance of the APG-FET biosensors for *E. coli* detection. a) The real-time current recording of the APG-FET upon exposure to *E. coli* with different concentrations: 10^2, 10^3, 10^4, 10^5, and 10^6 CFU mL^{-1}. b) The source–drain current change of APG-FETs versus *E. coli* concentration. The fitted line follows the Langmuir adsorption isotherm.

Table 1. Comparison of the sensing performance for various detection methods.

Method	Detection time	Bacteria	Detection limit	Sensitivity[a)]	Reference
Flow cytometry	5 min	*E. coli* and others	10^5 cells mL^{-1}	–	[36]
PCR test	4 h	*Listeria* and others	10^3 CFU mL^{-1}	–	[37]
Fluorescence	20 min	*E. coli*	50.2 CFU mL^{-1}	–	[38]
Antibody-modified G-FET	100 s	*E. coli*	10 CFU mL^{-1}	7.28×10^{-3}	[10]
Aptamer-modified G-FET	72 s	*E. coli*	10^2 CFU mL^{-1}	2.5×10^{-3}	This work

[a)]Sensitivity (S, μA per CFU mL^{-1}) defined as $S = \Delta I/c$, where ΔI is the net change of the source–drain current caused by *E. coli;* and c is the concentration of *E. coli*.

where ΔI_{ds} is the net change of the source–drain current caused by *E. coli*, $\Delta I_{ds,\,max}$ is the maximum net change in the source–drain current caused by *E. coli*, $C_{E.\,coli}$ is the *E. coli* concentration, and K_D is the equilibrium dissociation constant that can interpret the binding affinity of the probe–target complex. In Figure 6b, K_D is estimated as 700 CFU mL^{-1} from the fitting curve using Equation (3). This value is comparable to that of antibody-bacteria binding in previous studies ($K_D = 10^{2.6}$ CFU mL^{-1}),[41] indicating that the aptamer used in this study has a high affinity toward *E. coli*.

2.6. Selectivity and Stability

Selectivity is an important indicator to weigh the performance of biosensors. To investigate the specificity of AMG-FETs for *E. coli* detection, we tested the electrical response of APG-FETs to different bacteria including *E. coli* 8739, *E. coli* K12 *ER2925*, *Streptococcus mutans*, and *Staphylococcus saprophyticus*. The electrical response in this study is defined as $\Delta I_{ds}/I_{ds}$ where ΔI_{ds} and I_{ds} are the change in the source–drain current caused by the addition of bacteria and the source–drain current of the device before the addition, respectively. The selectivity evaluation of APG-FETs toward different bacteria is summarized in **Figure 7**a. The total response to *E. coli* 8739 (13.06%) is significantly larger than that to *E. coli* K12 *ER2925* (2.14%), *S. mutans* (–0.83%), and *S. saprophyticus* (–0.69%) when the concentrations of these bacteria are kept the same. The response of APG-FETs to the other three bacteria is weak. Exposure to *E. coli* K12 *ER2925* results in a slight current increase, which is attributed to the possibility that the binding site of the aptamer may be less expressed on the surface of *E. coli* K12 *ER2925* than that on the surface of *E. coli* 8739. The current decreases of the device caused by *S. mutans* and *S. saprophyticus* are because these two are Gram-positive bacteria; the positively charged bacterial cell wall in PBS buffer (pH = 7.2) could cause the decrease of hole density and hence the device current. These results further indicate that the response of APG-FETs is caused by the aptamer-bacteria binding and the aptamer-modified G-FETs can be used as the platform for bacteria detection with high selectivity.

Stability is another concern to evaluate the quality of a biosensor. To explore the stability of *E. coli* biosensors, the APG-FETs were stored in PBS buffer solution (pH = 7.2) at three representative temperatures: 4 °C (common temperature for sample storage), 25 °C (room temperature), and 40 °C (high temperature). For each temperature, three APG-FETs were used to investigate the electrical response upon exposure to *E. coli* solution in each week. As shown in Figure 7b, no significant changes of the response of all APG-FETs to bacteria were observed when the APG-FETs were kept at 4 °C (12.95 ± 0.19%) for six weeks. The same phenomena were observed for 25 °C (12.97 ± 0.19%) and 40 °C (12.89 ± 0.16%). Moreover, the response from the APG-FET devices, which were kept for

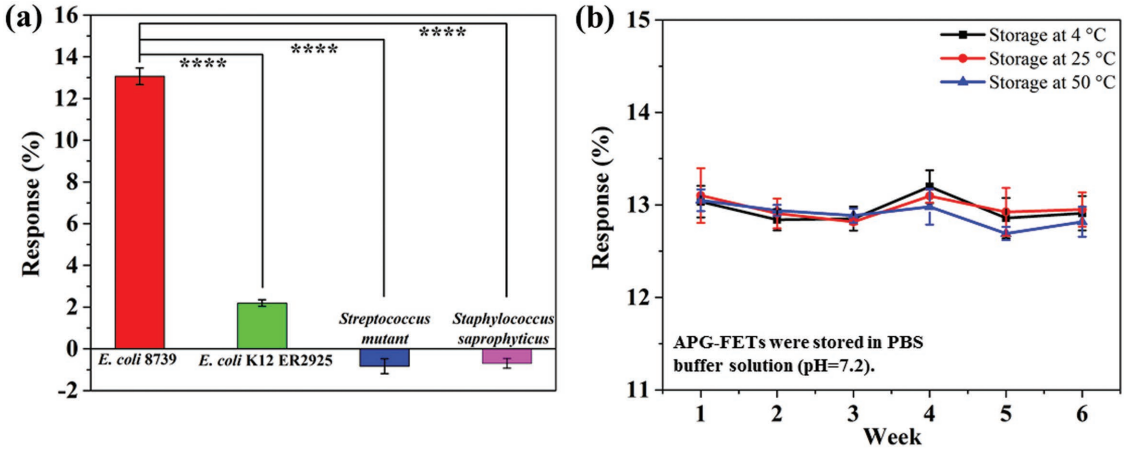

Figure 7. a) The response of APG-FETs to different bacteria: *E. coli* K12 *ER2925*, *E. coli* 8739, *S. mutans*, and *S. saprophyticus*. Results are given as mean ± standard derivation (SD), $n = 4$, ****$p < 0.0001$. b) The stability of APG-FET biosensors. The biosensors are stored in PBS buffer (pH = 7.2) for six weeks at different temperature (4, 25, and 40 °C).

the same time at different temperatures, shows only a small fluctuation from 12.82 ± 0.20% to 13.09 ± 0.14%. All of these results suggest excellent stability of our APG-FET biosensors. We attribute this stability to the inherent stability of the aptamer when it was stored for a long time (six weeks) at these temperatures.

3. Conclusions

We have demonstrated a reliable bacterial biosensor by using the APG-FET. Graphene was employed as the sensing material to fabricate the G-FET devices due to its excellent electronic properties and large specific area. As the sensing probe, the pyrene-tagged DNA aptamer toward *E. coli* was used to functionalize the G-FETs for the detection of *E. coli* with high sensitivity. The aptamer is easily modified and stable in harsh conditions. The binding of the negatively charged *E. coli* through the conformational change of the DNA aptamer increased the hole carrier density in graphene during the detection process. The detection mechanism is ascribed to the *E. coli*-induced electrostatic gating. The binding of negatively charged *E. coli* induces holes in graphene, which are pumped into the graphene channel from the contact electrodes. Quantitative analysis revealed that the APG-FETs exhibit a concentration-dependent response to *E. coli* 8739 with a low detection limit of 100 CFU mL^{-1}, which is obtained at the optimal gate voltage of 0.04 V. With this gate voltage, the largest electrical current change of 1.686 μA was obtained when the APG-FETs were exposed to 10^6 CFU mL^{-1} *E. coli*. Based on the Langmuir adsorption isotherm, a K_D of 700 CFU mL^{-1} was obtained, indicating very good affinity of the aptamer toward *E. coli*. The distinct selective response to the bacteria indicates that our biosensor can be used to distinguish *E. coli* 8739 from other bacteria strains. The excellent selectivity, affinity, and stability demonstrated here make the aptamer-modified graphene transistors a promising platform for the detection of various pathogens in environmental monitoring, public health, and food safety. More efforts are still needed to figure out the binding site on the bacterial surface and the effective part of the aptamer.

4. Experimental Section

Preparation of Bacterial Sample: *E. coli* ATCC 8739 and *E. coli* K12 *ER2925* (New England BioLabs) were cultured in the liquid nutrient broth medium. *S. mutans* ATCC 25175 was cultured in brain heart infusion broth, and *Lactobacillus acidophilus* ATCC 4356 was cultured in Lactobacilli MRS broth. All strains were cultured with a shaking incubator at 37 °C for 24 h. The crude bacterial culturing solution was diluted with 0.01× PBS buffer (pH 7.2) to different concentrations.

Synthesis of 2-Cyanoethyl (4-(pyren-1-yl) butyl) Diisopropylphosphoramidite (Pyrene Phosphoramidite, 1) Linker for Aptamer: 1H-tetrazole (28.2 mg, 0.4 mmol) and 2-cyanoethyl tetraisopropyl phosphoramidite (120 mg, 0.4 mmol) were first dissolved in 5 mL anhydrous CH_3CN under nitrogen atmosphere. Then 4-(1-pyrenyl) butanol (100 mg, 0.364 mmol) in 10 mL anhydrous CH_3CN was added dropwise to the above solution at 0 °C. Subsequently, the mixture was warmed to room temperature and stirred under nitrogen atmosphere overnight. At last, the solvent was removed by a rotary evaporator and the residue was dissolved in ethyl acetate and extracted by saturated $NaHCO_3$ solution. After being dried over anhydrous sodium sulfate, the resulting ethyl acetate solution was concentrated by a rotary evaporator and purified by silica gel chromatography (hexane:ethyl acetate = 7:3) to give 1 as a solid: yield 32.6% (56.3 mg). ^{1}H NMR ($CDCl_3$, 400 MHz) δ 1.16 (t, 12*H*), 1.80 (m, 2*H*), 1.96 (m, 2*H*), 2.56 (t, 2*H*), 3.38 (t, 2*H*), 3.59 (m, 2*H*), 3.78 (m, 2*H*), 7.88 (d, 1*H*) 7.97–8.03 (m, 3*H*), 8.08–8.18 (m, 4*H*), 8.29 (d, 1*H*); ^{13}C NMR ($CDCl_3$, 400 MHz) δ 20.18, 20.22, 27.96, 29.77, 30.98, 31.03, 33.02, 56.37, 56.45, 62.68, 62.80, 117.37, 123.36, 124.72, 124.80, 124.90, 125.01, 125.09, 125.84, 126.62, 127.24, 127.27, 127.52, 128.60, 129.83, 130.89, 131.43, 136.46; ^{31}P NMR ($CDCl_3$, 400 MHz) δ 147.30. ESI-MS *m/z* calcd for C29H35N2O2P $(M\text{-}H)^-$ 473.16, found 473.2.

Synthesis of the Pyrene-Tagged DNA Aptamer for E. coli Detection: The as-prepared pyrene derivative pyrene phosphoramidite was coupled into the DNA aptamer to anchor the aptamer onto the graphene surface. As a spacer, four thymine bases were introduced to link the DNA aptamer and the pyrene derivate. The sequence of the PTDA toward *E. coli* is listed here: 5′-(pyrene derivate)-TTTT-GCA ATG GTA CGG TAC TTC CCC ATG AGT GTT GTG AAA TGT TGG GAC ACT AGG TGG CAT AGA GCC GCA AAA GTG CAC GCT ACT TTG CTA A-3′. The detailed synthesis is shown in the Supporting Information.

Statistical Analysis: Experimental data are expressed as the mean ± standard derivation (SD) in Figure 7a (n = 4) and in Figure S10d, Supporting Information, (n = 10). The statistical significance of differences between mean values was determined using one-way ANOVA followed by *t*-test for analysis of variance, where the significance was evaluated for $p < 0.0001$. The software used for statistical analysis is GraphPad Prism 6.02.

Supporting Information

Supporting Information is available from the Wiley Online Library or from the author.

Acknowledgements

This research is supported by the GRF grant from the Research Grant Council of the Hong Kong Special Administrative Region Government (CityU 11205514 and CityU 11205815), National Natural Science of China (21574109), Health and Medical Research Fund (03141076) and CityU Internal Funding (7004655 and 9680104).

Conflict of Interest

The authors declare no conflict of interest.

Keywords

biosensors, detection, DNA aptamers, *Escherichia coli*, graphene transistors

Received: June 13, 2017
Revised: July 8, 2017
Published online:

[1] W. F. Law, N. S. Ab. Mutalib, K. G. Chan, L. H. Lee, *Front. Microbiol.* **2014**, *5*, 770.
[2] P. M. Wehrli, E. Lindberg, O. Svensson, A. Sparén, M. Josefson, R. H. Dunstan, *J. Chemom.* **2014**, *28*, S681.
[3] S. Liu, X. F. Guo, *NPG Asia Mater.* **2012**, *4*, e23.
[4] A. Q. Zhang, C. M. Lieber, *Chem. Rev.* **2016**, *116*, 215.

[5] B. B. Zhan, C. Li, J. Yang, G. Jenkins, W. Huang, X. C. Dong, *Small* **2014**, *10*, 4042.
[6] S. J. Park, O. S. Kwon, S. H. Lee, H. S. Song, T. H. Park, J. Jang, *Nano Lett.* **2012**, *12*, 5082.
[7] G. F. Wu, X. Tang, M. Meyyappan, K. W. C. Lai, *Appl. Surf. Sci.* **2017**, *425*, 713.
[8] K. Geim, K. S. Novoselov, *Nat. Mater.* **2007**, *6*, 183.
[9] Y. X. Huang, X. C. Dong, Y. X. Liu, L.-J. Li, P. Chen, *J. Mater. Chem.* **2011**, *21*, 12358.
[10] J. B. Chang, S. Mao, Y. Zhang, S. M. Cui, G. H. Zhou, X. G. Wu, C.-H. Yang, J. H. Chen, *Nanoscale* **2013**, *5*, 3620.
[11] K.-M. Song, S. Lee, C. Ban, *Sensors* **2012**, *12*, 612.
[12] A. D. Ellington, J. W. Szostak, *Nature* **1990**, *346*, 818.
[13] C. Tuerk, L. Gold, *Science* **1990**, *249*, 505.
[14] H. Qu, A. T. Csordas, J. P. Wang, S. S. Oh, M. S. Eisenstein, H. T. Soh, *ACS Nano* **2016**, *10*, 7558.
[15] J. H. An, S. J. Park, O. S. Kwon, J. Bae, J. Jang, *ACS Nano* **2013**, *7*, 10563.
[16] A. Mokhtarzadeh, J. E. Dolatabadi, K. Abnous, M. de la Guardia, M. Ramezani, *Biosens. Bioelectron.* **2015**, *68*, 95.
[17] Y. L. Zhang, Y. Huang, J. H. Jiang, G. L. Shen, R. Q. Yu, *J. Am. Chem. Soc.* **2007**, *129*, 15448.
[18] E. Sheikhzadeh, M. Chamsaz, A. P. F. Turner, E. W. H. Jager, V. Beni, *Biosens. Bioelectron.* **2016**, *80*, 194.
[19] S. M. Nimjee, C. P. Rusconi, B. A. Sullenger, *Annu. Rev. Med.* **2005**, *56*, 555.
[20] Y. S. Kim, M. Y. Song, J. Jurng, B. C. Kim, *Anal. Biochem.* **2013**, *436*, 22.
[21] W. Y. Fu, L. Jiang, E. P. van Geest, L. M. C. Lima, G. F. Schneider, *Adv. Mater.* **2017**, *29*, 1603610.
[22] X. P. A. Gao, G. F. Zheng, C. M. Lieber, *Nano Lett.* **2010**, *10*, 547.
[23] N. C. S. Vieira, J. Borme, G. Machado Jr., F. Cerqueira, P. P. Freitas, V. Zucolotto, N. M. R. Peres, P. Alpuim, *J. Phys. Condens. Matter.* **2016**, *28*, 085302.
[24] C. Caillier, D.-K. Ki, Y. Lisunova, I. Gaponenko, P. Paruch, A. F. Morpurgo, *Nanotechnology* **2013**, *24*, 405201.
[25] Y. H. Kwak, D. S. Choi, Y. N. Kim, H. Kim, D. H. Yoon, S. S. Ahn, J. W. Yang, W. S. Yang, S. Seo, *Biosens. Bioelectron.* **2012**, *37*, 82.
[26] C. Reiner-Rozman, M. Larisika, C. Nowak, W. Knolla, *Biosens. Bioelectron.* **2015**, *70*, 21.
[27] C. T. Lin, P. T. K. Loan, T. Y. Chen, K. K. Liu, C. H. Chen, K. H. Wei, L. J. Li, *Adv. Funct. Mater.* **2013**, *23*, 2301.
[28] C. J. Shearer, A. D. Slattery, A. J. Stapleton, J. G. Shapter, C. T. Gibson, *Nanotechnology* **2016**, *27*, 125704.
[29] J. Liu, T. Wei, J. Zhao, Y. Y. Huang, H. Deng, A. Kumar, C. X. Wang, Z. C. Liang, X. W. Ma, X. J. Liang, *Biomaterials* **2016**, *91*, 44.
[30] C. Y. Wang, X. Y. Cui, Y. Li, H. B. Li, L. Huang, J. Bi, J. Luo, L. Q. Ma, W. Zhou, Y. Cao, B. G. Wang, F. Miao, *Sci. Rep.* **2016**, *6*, 21711.
[31] Y. N. Chen, Z. P. Michael, G. P. Kotchey, Y. Zhao, A. Star, *ACS Appl. Mater. Interfaces* **2014**, *6*, 3805.
[32] W. Jiang, A. Saxena, B. Song, B. B. Ward, T. J. Beveridge, S. C. B. Myneni, *Langmuir* **2004**, *20*, 11433.
[33] E. E. Ferapontova, E. M. Olsen, K. V. Gothelf, *J. Am. Chem. Soc.* **2008**, *130*, 4256.
[34] Y. Xiao, A. A. Lubin, A. J. Heeger, K. W. Plaxco, *Angew. Chem.* **2005**, *117*, 5592.
[35] M. Zuker, *Nucl. Acids Res.* **2003**, *31*, 3406.
[36] H. Mohr, B. Lambrecht, A. Bayer, H. P. Spengler, S. B. Nicol, T. Montag, T. H. Müller, *Transfusion* **2006**, *46*, 41.
[37] M. Schmidt, *ISBT Sci. Ser.* **2009**, *4*, 80.
[38] P. Qi, D. Zhang, Y. Sun, Y. Wan, *Anal. Methods* **2016**, *8*, 3339.
[39] M. P. Starr, H. Stolp, H. G. Trüper, A. Balows, H. G. Schlegel, *Springer Sci. Business Media* **1981**, *1*, 6.
[40] B. Y. Lee, M. G. Sung, J. Lee, K. Y. Baik, Y. K. Kwon, M. S. Lee, S. Hong, *ACS Nano* **2011**, *5*, 4373.
[41] A. Chrouda, M. Braiek, K. B. Rokbani, A. Bakhrouf, A. Maaref, N. Jaffrezic-Renault, *ISRN Electrochem.* **2013**, *2013*, 9.

